Available online at www.sciencedirect.com
SCIENCE DIRECT®
Journal of Sound and Vibration 277 (2004) 919–930
JOURNAL OF SOUND AND VIBRATION
www.elsevier.com/locate/jsvi

Vibration analysis of a torus–cylinder shell assembly

D. Redekop*

Department of Mechanical Engineering, University of Ottawa, Ottawa, Ont., Canada K1N 6N5

Received 3 April 2003; accepted 20 September 2003

Abstract

Differential equations based on the Sanders–Budiansky theory are expressed in a general form for the linear vibration analysis of thin isotropic shells. The general equations are applied to toroidal and cylindrical shells and to a torus–cylinder shell assembly (pipe bend). Solutions to the equations are set up using the differential quadrature method. Sample results obtained for the cylindrical shell are compared with results given in the literature. Further results are given for some standard-size 90° pipe bends, and these results are compared with finite element results. The paper ends with an appropriate set of conclusions.
© 2003 Published by Elsevier Ltd.

1. Introduction

Shell assemblies consisting of two or more simple plate and/or shell components are frequently encountered in vibration analysis [1–6]. Structures such as these have application in the aircraft, shipbuilding, and pressure vessel industries, among others. Analytical solutions for such structures are useful either as primary solutions or as a means to confirm results found using the finite element method (FEM).

The formulation of analytical vibration solutions for shell assemblies poses a difficult problem for researchers. The standard approach involves setting up solutions for the individual components and then satisfying continuity conditions on lines of connection between components. A complication arises when the various shell components find natural description in different physical co-ordinate systems.

Analysis of such assemblies has been carried out using a variety of methods, including the receptance method [1] and the differential quadrature method (DQM) [3,6]. The latter method due to its implicit use of high order functions can offer great accuracy for relatively small

*Fax: +1-613-562-5177.
E-mail address: dredekop@tesla.cc.uottawa.ca (D. Redekop).

0022-460X/$ - see front matter © 2003 Published by Elsevier Ltd.
doi:10.1016/j.jsv.2003.09.034

computational effort. A recent paper by Chen et al. [6] indicated some difficulties with the DQM for multi-domain problems, and explored the use of the differential quadrature element method for such problems. The difficulties cited were numerical ones arising from differences in the order of terms in the equations sets.

In the present work, a single set of governing equations is obtained for the vibration analysis of a thin isotropic shell of arbitrary geometry. Specialization of the equations for specific shell geometries will involve terms that are of similar order. The linear form of the Sanders–Budiansky theory [10,11] is used to set up the equations, and the DQM is used to obtain solutions. Vibration analyses are then conducted for individual toroidal and cylindrical shells, as well as for a torus–cylinder shell assembly (pipe bend) [7–9]. Comparison is made with results from the FEM. The paper ends with a set of conclusions about the current approach, and the results obtained.

2. Geometry

A governing set of equations is developed for a thin shell of arbitrary mid-surface geometry. The mid-surface is described by a radius vector $\mathbf{r} = \mathbf{r}(q_1, q_2)$, where q_1, q_2 form an orthogonal co-ordinate system. The Lamé parameters of the shell are given by α_1, α_2, and the curvatures by k_1, k_2.

The shell assembly studied in this work is a pipe bend (Fig. 1), consisting of a 90° elbow (toroidal shell) and a straight pipe (cylindrical shell), joined at an interface BC. The elbow has a bend radius R and the pipe has a length L. The two components have a common radius r of cross-section, and a common thickness, h. The elbow is clamped at its base and the pipe is free at its far end.

The geometric parameters for a toroidal shell (Fig. 2) are given by

$$q_1 = \eta = \phi/\gamma, \quad q_2 = \theta, \quad \alpha_{1t} = r\zeta, \quad \alpha_{2t} = r, \quad k_{1t} = \cos\theta/(R\zeta), \quad k_{2t} = 1/r, \tag{1}$$

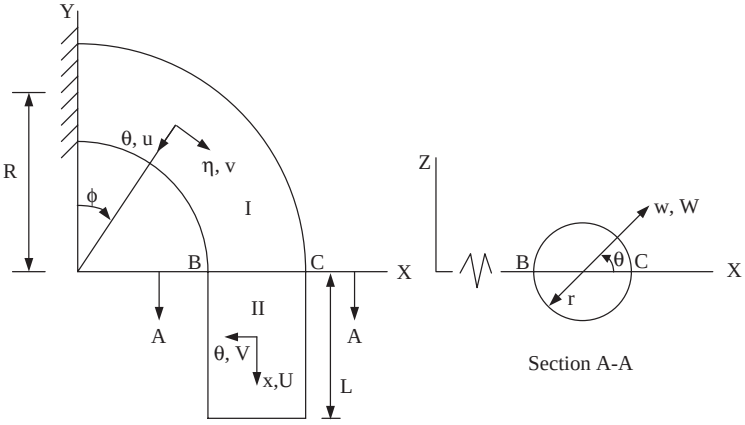

Fig. 1. Pipe bend.

where $\gamma = r/R$, $\zeta = 1 + \gamma \cos\theta$, ϕ is the longitudinal angular measure, and θ the circumferential angular measure. For a cylindrical shell, the geometric parameters are

$$q_1 = x/r, \quad q_2 = \theta, \quad \alpha_{1c} = r, \quad \alpha_{2c} = r, \quad k_{1c} = 0, \quad k_{2c} = 1/r, \tag{2}$$

where x is a local axial co-ordinate, while θ is again the circumferential angular measure. The subscripts t and c in Eqs. (1) and (2) and in subsequent equations refer to the toroidal and cylindrical shell components, respectively.

The boundary conditions at the base of the elbow are

$$u_t = 0, \quad v_t = 0, \quad w_t = 0, \quad k_{1t}u_t - w_{t,1}/\alpha_{1t} = 0, \tag{3}$$

where u_t, v_t, and w_t are the elbow displacement components in the η, θ, and normal directions respectively (Fig. 3), and $w_{t,1}$ represents the derivative in the longitudinal (η) direction. The far end of the pipe is free and, thus, zero-force boundary equations must be satisfied. According to the Sanders–Budiansky shell theory [10,11], the conditions are

$$N_{1c} = 0, \quad T_{1c} \equiv N_{12c} + \tfrac{1}{2}(3k_{2c} - k_{1c})M_{12c} = 0, \tag{4}$$

$$S_{1c} \equiv \frac{1}{\alpha_{1c}\alpha_{2c}}[(\alpha_{2c}M_{1c})_{,1} + (\alpha_{1c}M_{12c})_{,2} + \alpha_{1c,2}M_{12c} - \alpha_{2c,1}M_{12c}] + \frac{1}{\alpha_{2c}}M_{12c,2} = 0,$$

$$M_{1c} = 0,$$

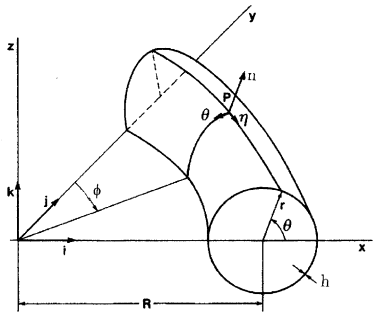

Fig. 2. Toroidal shell geometry.

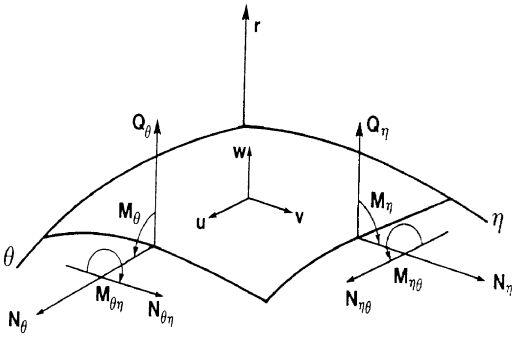

Fig. 3. Toroidal displacements and resultants.

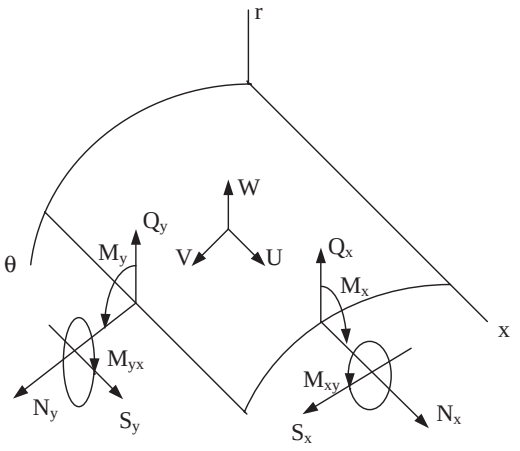

Fig. 4. Cylindrical displacements and resultants.

where the $(\cdots)_{,1}$ and $(\cdots)_{,2}$ indicate differentiation with respect to the q_1 and q_2 variables, and, for a cylindrical shell, $N_{1c} = N_x$, $N_{12c} = N_{x\theta}$, $M_{12c} = M_{x\theta}$, $M_{1c} = M_x$, and $M_{2c} = M_\theta$. The convention for the stress resultants in the pipe is shown in Fig. 4. The resultants can be expressed in terms of the displacement components using the geometric and constitutive relations given in the following section.

Campatibility at the interface BC necessitates continuity of both displacement and force. The continuity conditions to be satisfied are

$$u_t = u_c, \quad v_t = v_c, \quad w_t = w_c, \quad k_{1t}u_t - w_{t,1}/\alpha_{1t} = k_{1c}u_c - w_{c,1}/\alpha_{1c} \tag{5}$$

and

$$N_{1t} = N_{1c}, \quad T_{1t} = T_{1c}, \quad S_{1t} = S_{1c}, \quad M_{1t} = M_{1c}, \tag{6}$$

where the resultants are defined with the help of Eqs. (4).

3. Sanders–Budiansky shell theory

To determine the vibration characteristics of the shell components and shell assembly, the first order linear version of the Sanders–Budiansky shell theory [10,11] is used, in conjunction with the D'Alembert principle. The governing equations in this theory, expressed in terms of the stress resultants and displacements in an arbitrary co-ordinate system, are

$$\begin{aligned}
&(\alpha_2 N_1)_{,1} + (\alpha_1 N_{12})_{,2} + \alpha_{1,2} N_{12} - \alpha_{2,1} N_2 + k_1(\alpha_2 M_1)_{,1} + k_1(\alpha_1 M_{12})_{,2} + k_1 \alpha_{1,2} M_{12} \\
&\quad - k_1 \alpha_{2,1} M_2 + \tfrac{1}{2}\alpha_1[(k_1 - k_2)M_{12}]_{,2} = \alpha_1 \alpha_2 \rho h \ddot{u}_1, \\
&(\alpha_1 N_2)_{,2} + (\alpha_2 N_{12})_{,1} + \alpha_{2,1} N_{12} - \alpha_{1,2} N_1 + k_2(\alpha_1 M_2)_{,2} + k_2(\alpha_2 M_{12})_{,1} + k_2 \alpha_{2,1} M_{12} \\
&\quad - k_2 \alpha_{1,2} M_1 + \tfrac{1}{2}\alpha_2[(k_2 - k_1)M_{12}]_{,1} = \alpha_1 \alpha_2 \rho h \ddot{u}_2,
\end{aligned}$$

$$[(\alpha_2 M_1)_{,1}/\alpha_1]_{,1} + [(\alpha_1 M_{12})_{,2}/\alpha_1]_{,1} + [\alpha_{1,2} M_{12}/\alpha_1]_{,1} - [\alpha_{2,1} M_2/\alpha_1]_{,1} + [(\alpha_1 M_2)_{,2}/\alpha_2]_{,2} + [(\alpha_2 M_{12})_{,1}/\alpha_2]_{,2} + [\alpha_{2,1} M_{12}/\alpha_2]_{,2} - [\alpha_{1,2} M_1/\alpha_2]_{,2} - \alpha_1\alpha_2(k_1 N_1 + k_2 N_2) = \alpha_1\alpha_2\rho h\ddot{w}, \quad (7)$$

where ρ is the mass density, and $\ddot{u}_1$, $\ddot{u}_2$, $\ddot{w}$ are the accelerations.

For the boundary and continuity conditions, an elastic law is required. In the Sanders–Budiansky shell theory, this is given by

$$\begin{aligned}
N_1 &= a_1 u_{1,1} + a_2 u_1 + a_3 u_{2,2} + a_4 u_2 + a_5 w,\\
N_2 &= a_6 u_{1,1} + a_7 u_1 + a_8 u_{2,2} + a_9 u_2 + a_{10} w,\\
N_{12} &= a_{11} u_{1,2} + a_{12} u_1 + a_{13} u_{2,1} + a_{14} u_2,\\
M_1 &= a_{15} u_{1,1} + a_{16} u_1 + a_{17} u_{2,2} + a_{18} u_2 + a_{19} w_{,11} + a_{20} w_{,1} + a_{21} w_{,22} + a_{22} w_{,2},\\
M_2 &= a_{23} u_{1,1} + a_{24} u_1 + a_{25} u_{2,2} + a_{26} u_2 + a_{27} w_{,11} + a_{28} w_{,1} + a_{29} w_{,22} + a_{30} w_{,2},\\
M_{12} &= a_{31} u_{1,2} + a_{32} u_1 + a_{33} u_{2,1} + a_{34} u_2 + a_{35} w_{,1} + a_{36} w_{,2} + a_{37} w_{,12},\\
Q_1 &= [(\alpha_2 M_1)_{,1} + (\alpha_1 M_{12})_{,2} + \alpha_{1,2} M_{12} - \alpha_{2,1} M_2]/(\alpha_1\alpha_2),\\
Q_2 &= [(\alpha_1 M_2)_{,2} + (\alpha_2 M_{12})_{,1} + \alpha_{2,1} M_{12} - \alpha_{1,2} M_1]/(\alpha_1\alpha_2),
\end{aligned} \quad (8)$$

where the a_1–a_{37} are known functions of the geometric and material properties of the shell.

Substitution of the elastic law (8) into the governing equations (7) and into the boundary-continuity relations (3)–(6) leads to domain and boundary equations in terms of displacements that govern the problem. The combined set of differential equations contains as the unknowns the displacement components and the natural frequency. The solution of this equation set using the DQM is now considered.

4. Differential quadrature method

The first step in the DQM approach [12,13] is the definition of a grid of sampling points covering the domain, including the boundary. The spacing of sampling points may be even, but more generally is irregular. The three displacement components at each of the sampling points constitute the principal unknowns of the problem.

The second step in the DQM approach is the replacement, in domain and boundary-continuity equations, of derivatives with series that contain the displacements at the sampling points and weighting coefficients. This step enables a conversion of the problem from one of differential equations to one of linear equations. The rth derivative of a generic function of a single variable $f(x)$ at the sampling point x_i is represented as

$$\left.\frac{\mathrm{d}^r f(x)}{\mathrm{d}x^r}\right|_{x_i} = \sum_{h=1}^{M} A_{ih}^{(r)} f(x_h), \quad (9)$$

where the $A_{ih}^{(r)}$ are the weighting coefficients of the rth order derivative in the x direction for the ith sampling point, $f(x_h)$ is the value of $f(x)$ at the sampling point position x_h, and M is the number of sampling points in the x direction. The $(r+s)$th partial derivative of a generic function of two

variables $g(x,y)$ at the sampling point x_i, y_j is represented as

$$\left.\frac{\partial^{(r+s)} g(x,y)}{\partial x^r \partial y^s}\right|_{x_i,y_j} = \sum_{h=1}^{M} A_{ih}^{(r)} \sum_{k=1}^{N} B_{jk}^{(s)} g(x_h, y_k), \tag{10}$$

where $B_{jk}^{(s)}$ and N are weighting coefficients and number of terms in the series for the y direction, and $g(x_h, y_k)$ is the value of $g(x,y)$ at the sampling point position x_h, y_k.

In the DQM, the weighting coefficients are determined a priori for a preselected grid, with the aid of selected trial functions. In the present study, for the longitudinal direction, the well-known Chebyshev–Gauss–Lobatto spacing of sampling points with 'delta points' was adopted, together with polynomial trial functions. For such a scheme, explicit formulas for the weighting coefficients $A_{ih}^{(r)}$ are available [13]. For the circumferential direction, a system of evenly spaced sampling points was adopted, together with trigonometric trial functions. Explicit formulas are then available for the $B_{jk}^{(s)}$ weighting coefficients [13].

In the torus–cylinder assembly problem separate grids of sampling points were defined for each of the components. These grids overlapped on the interface BC, and lines of 'delta points' were situated on either side of the interface. The equations written for the interface and 'delta point' sampling points were the set of continuity conditions of Eqs. (5) and (6).

Use of the quadrature rules (9)–(10) for the derivatives in the domain of the governing differential equations leads to the transformed DQM vibration equations

$$\begin{aligned}
&c_1 \sum A_{ih}^{(2)} U_{hj} + c_2 \sum A_{ih}^{(1)} U_{hj} + c_3 \sum B_{jk}^{(2)} U_{ik} + c_4 \sum B_{jk}^{(1)} U_{ik} + c_5 U_{ij} \\
&\quad + c_6 \sum A_{ih}^{(1)} V_{hj} + c_7 \sum B_{jk}^{(1)} V_{ik} + c_8 \sum A_{ih}^{(1)} \sum B_{jk}^{(1)} V_{hk} + c_9 V_{ij} \\
&\quad + c_{10} \sum A_{ih}^{(3)} W_{hj} + c_{11} \sum A_{ih}^{(2)} W_{hj} + c_{12} \sum A_{ih}^{(1)} W_{hj} + c_{13} \sum B_{jk}^{(2)} W_{ik} + c_{14} \sum B_{jk}^{(1)} W_{ik} \\
&\quad + c_{15} \sum A_{ih}^{(1)} \sum B_{jk}^{(2)} W_{hk} + c_{16} \sum A_{ih}^{(1)} \sum B_{jk}^{(1)} W_{hk} + c_{17} W_{ij} = \lambda U_{ij},
\end{aligned} \tag{11}$$

$$\begin{aligned}
&c_{18} \sum A_{ih}^{(1)} U_{hj} + c_{19} \sum B_{jk}^{(1)} U_{ik} + c_{20} \sum A_{ih}^{(1)} \sum B_{jk}^{(1)} U_{hk} + c_{21} U_{ij} \\
&\quad + c_{22} \sum A_{ih}^{(2)} V_{hj} + c_{23} \sum A_{ih}^{(1)} V_{hj} + c_{24} \sum B_{jk}^{(2)} V_{ik} + c_{25} \sum B_{jk}^{(1)} V_{ik} + c_{26} V_{ij} \\
&\quad + c_{27} \sum A_{ih}^{(2)} W_{hj} + c_{28} \sum A_{ih}^{(1)} W_{hj} + c_{29} \sum B_{jk}^{(3)} W_{ik} + c_{30} \sum B_{jk}^{(2)} W_{ik} + c_{31} \sum B_{jk}^{(1)} W_{ik} \\
&\quad + c_{32} \sum A_{ih}^{(2)} \sum B_{jk}^{(1)} W_{hk} + c_{33} \sum A_{ih}^{(1)} \sum B_{jk}^{(1)} W_{hk} + c_{34} W_{ij} = \lambda V_{ij},
\end{aligned}$$

$$\begin{aligned}
&c_{35} \sum A_{ih}^{(3)} U_{hj} + c_{36} \sum A_{ih}^{(2)} U_{hj} + c_{37} \sum A_{ih}^{(1)} U_{hj} + c_{38} \sum B_{jk}^{(2)} U_{ik} + c_{39} \sum B_{jk}^{(1)} U_{ik} \\
&\quad + c_{40} \sum A_{ih}^{(1)} \sum B_{jk}^{(2)} U_{hk} + c_{41} \sum A_{ih}^{(1)} \sum B_{jk}^{(1)} U_{hk} + c_{42} U_{ij} \\
&\quad + c_{43} \sum A_{ih}^{(2)} V_{hj} + c_{44} \sum A_{ih}^{(1)} V_{hj} + c_{45} \sum B_{jk}^{(3)} V_{ik} + c_{46} \sum B_{jk}^{(2)} V_{ik} + c_{47} \sum B_{jk}^{(1)} V_{ik} \\
&\quad + c_{48} \sum A_{ih}^{(2)} \sum B_{jk}^{(1)} V_{hk} + c_{49} \sum A_{ih}^{(1)} \sum B_{jk}^{(1)} V_{hk} + c_{50} V_{ij}
\end{aligned}$$

$$+ c_{51}\sum A_{ih}^{(4)}W_{hj} + c_{52}\sum A_{ih}^{(3)}W_{hj} + c_{53}\sum A_{ih}^{(2)}W_{hj} + c_{54}\sum A_{ih}^{(1)}W_{hj}$$
$$+ c_{55}\sum B_{jk}^{(4)}W_{ik} + c_{56}\sum B_{jk}^{(3)}W_{ik} + c_{57}\sum B_{jk}^{(2)}W_{ik} + c_{58}\sum B_{jk}^{(1)}W_{ik}$$
$$+ c_{59}\sum A_{ih}^{(2)}\sum B_{jk}^{(2)}W_{hk} + c_{60}\sum A_{ih}^{(2)}\sum B_{jk}^{(1)}W_{hk} + c_{61}\sum A_{ih}^{(1)}\sum B_{jk}^{(2)}W_{hk}$$
$$+ c_{62}\sum A_{ih}^{(1)}\sum B_{jk}^{(1)}W_{hk} + c_{63}W_{ij} = \lambda W_{ij}.$$

where $\lambda = \rho h\omega^2$, and ω is the natural frequency in Hz. The c_i, $i = 1, 2, \ldots, 63$ in Eq. (11) signify known functions of the geometric co-ordinates and the material properties, which include E, the elastic modulus, and v, the Poisson ratio. The U_{ij}, V_{ij}, W_{ij} are the displacement components at the sampling point i,j, and the summations extend over the full set of sampling points in the appropriate co-ordinate direction. It is understood that these equations will be enforced at the various sampling points of a pre-selected grid. DQM equations for the boundary-continuity conditions to be enforced at the boundary-continuity points may similarly be written.

The assembly of the domain and boundary-continuity relations yields a matrix equation of the form

$$\begin{bmatrix} K_{bb} & K_{bd} \\ K_{db} & K_{dd} \end{bmatrix} \begin{Bmatrix} \Delta_b \\ \Delta_d \end{Bmatrix} = \lambda \begin{bmatrix} 0 & 0 \\ 0 & I \end{bmatrix} \begin{Bmatrix} \Delta_b \\ \Delta_d \end{Bmatrix}. \tag{12}$$

The sub-matrices $[K_{bb}]$ and $[K_{bd}]$ of the 'stiffness' matrix stem from the boundary-continuity conditions, while the sub-matrices $[K_{db}]$ and $[K_{dd}]$ stem from the domain equations. Sub-matrix $[I]$ is the identity matrix. The vector $\{\Delta_b\}$ contains the displacements at the boundary-continuity points, while the vector $\{\Delta_d\}$ represents the displacements at the domain points. Solution of this equation yields the natural frequencies of vibration of the shell or shell assembly, as well as the mode shapes.

The theory for vibration of a clamped–clamped toroidal shell, a clamped–free cylindrical shell, and a clamped–free pipe bend was coded in the two-variable DQM programs sanbudt.m, sanbudc.m, and benvib.m, respectively. Earlier comparisons of computer times between the DQM and FEM have indicated the effectiveness of the DQM solution [12]. Results from the mentioned DQM programs are presented in the following.

5. Finite element method

The commercial FEM program NE-NASTRAN [14] was used to provide an alternate solution to the vibration problem. A flat four-noded 24 degree-of-freedom shell element is available in this program for the solution of linear shell vibration problems. Manual meshing was carried out with element numbers chosen to give nearly square elements. The modelling accounted for the full geometry, with no account made of the symmetry.

6. Validation

A comparison with previous work was made for the case of a cylindrical shell with clamped–free support conditions. The study was for the following values of the geometric and material parameters: $L = 0.5112$ m, $r = 0.216$ m, $h = 0.0015$ m, $E = 0.183\text{e}12$ Pa, $v = 0.3$, $\rho = 7492$ kg/m^3. These values corresponded to a cylindrical shell studied by Chung [15] using a series approach and by Ganesan and Sivadas [16] using the FEM.

A comparison of results for the first 10 natural frequencies is given in Table 1. The $\hat{m}$, $\hat{n}$ values in the table refer to the mode numbers in the axial and circumferential directions, as given in Ref. [16]. The present values are those obtained using the sanbudc.m DQM program with a mesh consisting of 27 longitudinal sampling points and 28 circumferential points. Convergence of the solution is discussed further in the following section. The table indicates that differences between the present results and the previous FEM results [16] are less than 1%, up to the eight natural frequency. Differences with the previous series solution [15] are less than 2%, up to the tenth natural frequency.

7. Results

Natural frequencies of vibration are determined for three pipe bends of standard geometry. Details of the dimensions are given in Table 2. These bends are similar in geometry to ones studied by Basaraju and Lee [8], but involve only one straight pipe, the length of which is one pipe diameter. The results were obtained using the following values for the material properties: $E = 0.207\text{e}12$ Pa, $v = 0.3$, $\rho = 7800$ kg/m^3.

Frequencies are first obtained for the individual toroidal and cylindrical components of each of the three pipe bends. For the toroidal components, clamped–clamped boundary conditions are assumed, while for the cylindrical ones clamped–free conditions are used. Results for the first five natural frequencies of the components as determined from both the FEM and DQM are presented in Table 3. Results from one 'fine' FEM mesh and for three DQM meshes are given. In the table, the numbers for the meshes indicate elements or sampling points in the longitudinal and

Table 1
Validation study

Root	$\hat{m}$, $\hat{n}$	Ref. [15]	Ref. [16]	Present
1	1, 4	171.8	173.6	173.24
2	1, 5	199.2	202.3	202.29
3	1, 3	223.3	224.4	223.78
4	1, 6	268.9	273.5	273.76
5	1, 7	361.9	370.1	368.76
6	1, 2	403.7	404.7	404.01
7	2, 6	447.0	448.7	445.81
8	2, 7	464.6	471.3	470.88
9	1, 8	472.5	490.3	481.56
10	2, 5	494.7	500.3	496.62

Table 2
Description of elbows

	Elbow	$R(m)$	$r(m)$	$h(m)$	$L(m)$	r/h	$H = hR/r^2$
1	ELB6A	0.2286	0.0858	0.00711	0.1716	12.1	0.221
2	ELB14B	0.5334	0.1730	0.00953	0.3460	18.2	0.170
3	ELB20A	0.7620	0.2492	0.00953	0.4984	26.1	0.117

Table 3
Component natural frequencies—convergence characteristics (Hz)

Model	Method	Mesh	Mode				
			1	2	3	4	5
6A-Tor	FEM	32×48	2271.770	2627.810	2913.290	3178.770	3422.830
	DQM-3	27×28	2273.076	2628.331	2920.583	3198.794	3441.326
	DQM-2	19×20	2273.077	2628.332	2920.583	3198.794	3441.326
	DQM-1	11×12	2272.648	2627.957	2921.473	3198.450	3440.829
6A-Cyl	FEM	20×64	1578.290	2016.920	2795.740	3524.030	4394.390
	DQM-3	27×28	1600.484	2085.321	2799.311	3626.575	4365.014
	DQM-2	19×20	1600.485	2085.322	2799.312	3626.575	4365.015
	DQM-1	11×12	1600.336	2081.834	2800.134	3622.559	4361.829
14B-Tor	FEM	36×44	967.993	1099.320	1169.130	1209.140	1294.320
	DQM-3	27×28	966.859	1096.121	1165.342	1204.963	1291.727
	DQM-2	19×20	966.856	1096.119	1165.342	1204.963	1291.727
	DQM-1	11×12	965.290	1095.005	1165.712	1205.828	1291.476
14B-Cyl	FEM	20×64	734.923	735.207	1199.640	1379.670	1811.120
	DQM-3	27×28	737.485	744.635	1210.153	1380.510	1833.520
	DQM-2	19×20	737.485	744.636	1210.154	1380.510	1833.520
	DQM-1	11×12	737.010	741.627	1206.376	1380.802	1831.320
20A-Tor	FEM	36×44	664.002	734.759	745.094	764.822	850.279
	DQM-3	27×28	662.308	730.608	739.893	759.333	840.838
	DQM-2	19×20	662.299	730.605	739.892	759.332	840.834
	DQM-1	11×12	661.569	727.903	741.023	765.289	837.540
20A-Cyl	FEM	20×64	405.137	494.177	596.214	926.977	954.883
	DQM-3	27×28	406.051	494.202	595.383	919.338	955.207
	DQM-2	19×20	406.052	494.202	595.384	919.339	955.207
	DQM-1	11×12	402.747	493.357	591.066	915.421	955.212

circumferential directions, respectively. For the FEM meshes, the element numbers represent an effort to obtain 'square' elements while, for the DQM meshes, the sampling point numbers represent an effort to give nearly the same order of function in the two co-ordinate directions.

For both the toroidal and cylindrical components, there is excellent agreement in results between the FEM and DQM for all three geometries (in inverted order). Differences for the

fundamental frequency are less than two percent, indicating accuracy in the derived equations and corresponding codes. The DQM solutions are very steady with increase in sampling points, permitting a converged accuracy of 5–6 figures without a loss of numerical stability.

Frequencies are next found for the torus–cylinder assemblies, i.e., the complete pipe bends. In these analyses, clamped support conditions are assumed at the toroidal end and free conditions at the cylindrical end. Results are given in Table 4 for the first five frequencies as determined by both the FEM and DQM. Results are given for three FEM meshes as well as three DQM meshes (in inverted order). The mesh sizes quoted indicate either elements or sample point numbers following the convention mentioned for Table 3.

For the pipe bends, close agreement is obtained in results between the FEM and DQM for all three geometries, with differences for the fundamental frequency less than five percent. In the FEM solution, convergence is seen to be monotonic. In the DQM results, in general, convergence with an increase in the number of sampling points is steady as well, except for ELB 6A, modes 1 and 2, ELB14B, modes 2 and 5, and ELB20A, modes 1 and 2. The DQM solution for the shell assembly is less stable than for the individual components, and tends to degrade if large number of sampling points are used. This tendency of the DQM solution has been noted by previous authors [6,12]. The solutions obtained, however, clearly are of accuracy suitable for engineering purposes.

The effect of changing the length of the cylindrical shell on the natural frequencies of the three pipe bends is shown in Table 5. Three cylindrical shell lengths are specified as $L_1 = 0.5L$, $L_2 = L$, and $L_3 = 1.5L$, where L represents the cylindrical shell length given in Table 2. The first five

Table 4
Assembly natural frequencies—convergence characteristics (Hz)

Model	Method	Tor + Cyl Mesh	Mode				
			1	2	3	4	5
ELB6A	FEM-1	$14 \times 22 + 7 \times 22$	335.5	350.8	752.5	763.3	1248.0
	FEM-2	$20 \times 32 + 10 \times 32$	333.9	349.4	740.5	750.8	1241.0
	FEM-3	$28 \times 44 + 14 \times 44$	327.4	342.5	721.1	730.9	1215.0
	DQM-3	$13 \times 14 + 13 \times 14$	335.1	356.5	725.4	734.4	1250.0
	DQM-2	$11 \times 12 + 11 \times 12$	337.0	352.9	723.4	733.8	1249.0
	DQM-1	$9 \times 10 + 9 \times 10$	330.1	353.0	712.4	721.6	1243.0
ELB14B	FEM-1	$16 \times 20 + 7 \times 20$	126.0	131.6	263.3	267.1	497.1
	FEM-2	$24 \times 30 + 10 \times 30$	125.3	130.8	258.4	262.1	492.5
	FEM-3	$32 \times 40 + 14 \times 40$	122.9	128.4	252.1	255.7	482.2
	DQM-3	$13 \times 14 + 13 \times 14$	126.6	132.5	250.7	254.9	494.9
	DQM-2	$11 \times 12 + 11 \times 12$	125.2	131.2	250.7	254.4	493.2
	DQM-1	$9 \times 10 + 9 \times 10$	122.5	132.0	242.7	246.1	492.0
ELB20A	FEM-1	$16 \times 20 + 7 \times 20$	76.7	79.9	141.9	144.4	318.1
	FEM-2	$24 \times 30 + 10 \times 30$	76.1	79.2	139.2	141.7	309.3
	FEM-3	$32 \times 40 + 14 \times 40$	75.9	79.0	138.3	140.7	305.9
	DQM-3	$13 \times 14 + 13 \times 14$	75.2	79.9	135.8	138.4	300.7
	DQM-2	$11 \times 12 + 11 \times 12$	75.7	79.0	134.1	137.1	298.8
	DQM-1	$9 \times 10 + 9 \times 10$	73.3	79.0	128.1	131.3	287.5

Table 5
Effect of changing cylindrical shell length L on natural frequencies (Hz)

Model	L	Method	Tor + Cyl Mesh	Mode				
				1	2	3	4	5
ELB6A	L_1	FEM	$28 \times 44 + 10 \times 44$	448.8	457.8	859.7	880.2	1609.0
		DQM	$11 \times 12 + 11 \times 12$	460.4	474.7	840.9	860.1	1614.0
	L_2	FEM	$28 \times 44 + 14 \times 44$	327.4	342.5	721.1	730.9	1215.0
		DQM	$13 \times 14 + 13 \times 14$	335.1	356.5	725.4	734.4	1250.0
	L_3	FEM	$24 \times 44 + 18 \times 44$	249.9	266.7	685.1	690.4	1019.0
		DQM	$13 \times 14 + 13 \times 14$	254.9	271.0	681.6	686.8	1032.0
ELB14B	L_1	FEM	$32 \times 40 + 10 \times 40$	164.6	167.9	306.6	313.3	609.7
		DQM	$11 \times 12 + 11 \times 12$	160.2	170.8	296.5	305.2	606.0
	L_2	FEM	$32 \times 40 + 14 \times 40$	122.9	128.4	252.1	255.7	482.2
		DQM	$13 \times 14 + 13 \times 14$	126.6	132.5	250.7	254.9	494.9
	L_3	FEM	$28 \times 36 + 20 \times 36$	94.8	101.1	231.5	233.4	408.3
		DQM	$13 \times 14 + 13 \times 14$	96.3	102.9	231.3	233.2	412.8
ELB20A	L_1	FEM	$32 \times 40 + 10 \times 40$	97.5	99.1	177.3	181.5	334.1
		DQM	$11 \times 12 + 11 \times 12$	97.4	97.4	171.0	178.8	332.8
	L_2	FEM	$32 \times 40 + 14 \times 40$	75.9	79.0	138.3	140.7	305.9
		DQM	$13 \times 14 + 13 \times 14$	75.2	79.9	135.8	138.4	300.7
	L_3	FEM	$28 \times 40 + 18 \times 40$	58.5	62.4	120.4	121.6	268.6
		DQM	$13 \times 14 + 13 \times 14$	58.6	62.6	117.8	119.0	269.8

natural frequencies as found by the FEM and DQM are given. There is again close agreement in the results. The table indicates that increasing the length of the cylindrical shell substantially reduces the natural frequencies.

8. Conclusions

General vibration equations have been obtained, which enable the analysis of isotropic shells of arbitrary geometry, and of shell assemblies. The specific cases of toroidal and cylindrical shells and a shell assembly consisting of a 90° elbow and a straight pipe are covered in detail. Results obtained for the cylindrical shell show excellent agreement with results given in the literature. Results for the two shell types and the shell assembly also compare well with finite element results. The study demonstrates the suitability of the differential quadrature method for the analysis of shell assemblies.

References

[1] D.T. Huang, W. Soedel, On the free vibrations of multiple plates welded to a cylindrical shell with special attention to mode pairs, *Journal of Sound and Vibration* 166 (1993) 315–339.

[2] W.L. Cleghorn, S.D. Yu, R.G. Fenton, Free flexural vibration of a plate–shell assembly, *Proceedings of the 15th Canadian Congress of Applied Mechanics* (*CANCAM95*), Victoria, Vol. 1, 1995, pp. 266–267.
[3] A.R. Kukreti, Z.A. Siddiqi, Analysis of fluid storage tanks including foundation-superstructure interaction using the DQM, *Applied Mathematical Modelling* 21 (1997) 193–205.
[4] R.M. Grice, R.J. Pinnington, A method for the vibration analysis of built-up structures, Part I: introduction and analytical analysis of the plate-stiffened beam, *Journal of Sound and Vibration* 230 (4) (2000) 825–849.
[5] Y.-S. Lee, M.-S. Yang, H.-S. Kim, J.-H. Kim, A study on the free vibration of the joined cylindrical–spherical shell structures, *Computers and Structures* 80 (2002) 2405–2414.
[6] W.L. Chen, A.G. Striz, C.W. Bert, High-accuracy plane stress and plate elements in the quadrature element method, *International Journal of Solids and Structures* 37 (2000) 627–647.
[7] J.F. Whatham, Pipe bend analysis by thin shell theory, *Journal of Applied Mechanics* 53 (1986) 173–180.
[8] C. Basavaraju, R.L. Lee, Stress distribution in elbow due to external moments using finite-element methodology, *American Society of Mechanical Engineers* PVP-249 (1993) 103–112.
[9] R. Kumar, M.A. Saleem, Bend angle effect on B_2 and C_2 stress indices for piping elbows, *Journal of Pressure Vessel Technology* 123 (2001) 226–231.
[10] J.L. Sanders Jr., Nonlinear theories for thin shells, *Quarterly of Applied Mathematics* 21 (1963) 21–36.
[11] B. Budiansky, Notes on nonlinear shell theory, *Journal of Applied Mechanics* 40 (1968) 393–401.
[12] C.W. Bert, M. Malik, Free vibration analysis of thin cylindrical shells by the differential quadrature method, *Journal of Pressure Vessel Technology* 118 (1996) 1–12.
[13] C. Shu, *Differential Quadrature and its Application in Engineering*, Springer, Berlin, 2000.
[14] Noran Engineering Inc., *NE/Nastran User's Manual*, V2.3, Noran Engineering Inc., Garden Grove, CA, 1996.
[15] H. Chung, Free vibration analysis of circular cylindrical shells, *Journal of Sound and Vibration* 74 (1981) 331–350.
[16] N. Ganesan, K.R. Sivadas, Free vibration of cantilever circular cylindrical shells with variable thickness, *Computers and Structures* 34 (1990) 669–677.